

Image Mosaicing from Uncalibrated Views of a Surface of Revolution

Carlo Colombo, Alberto Del Bimbo, Federico Pernici
Dipartimento di Sistemi e Informatica – Università di Firenze
Via Santa Marta 3, I-50139 Firenze, Italy
E-mail {colombo,delbimbo,pernici}@dsi.unifi.it

Abstract

We present a novel approach to obtain a mosaic image for the surface texture content of a surface of revolution (SOR) from a collection of uncalibrated views. The SOR scene constraint is used to calibrate each view and align the corresponding pictorial content into a global representation. Metric surface properties are extracted from each view by exploiting special properties of the imaged SOR geometry expressed in terms of homologies. Image alignment is achieved by projecting imaged surface elements onto a reference plane, and then registering them according to a translational motion model. This work extends previous research on calibrated scenes of right circular cylinders to the more general case of uncalibrated SOR scenes. Experimental results with images taken from the web demonstrate the effectiveness and the general applicability of the approach.

1 Introduction and Related Work

Image mosaicing consists in merging collections of images having a partially overlapping content. The process can be decomposed into three main steps. First, the transformations relating each image coordinate system with a reference one are computed; the images are then warped according to the associated transformations, and finally aligned to each other to compose a single mosaic image.

Several approaches were proposed in the literature, mainly differing in the alignment methods adopted and in the class of warping transformations considered [8], [20]. The most common warping transformations fall into the class of projective and affine planar parametric models, related to special camera motions (e.g., rotations only) and/or scene geometry (e.g., planar scenes) [15], [7]. A typical example is that of panoramic mosaics, which are obtained either with a pan-only or with a pan/tilt camera, and are further warped onto a cylindrical or a spherical manifold, respectively, to obtain a 360° panorama [12], [2], [18]. A general technique for projecting an image mosaic onto a curved manifold according to camera motion is developed in [19].

If camera motion is unconstrained but the scene is planar, standard parametric models (i.e., planar homographies) can still be used for mosaicing purposes. This is not the case for general curved scenes, that require image transformation models which are more complex than homographies and are typically—even if not always [17]—non parametric. Due to its intrinsic difficulties, the problem of curved scene mosaicing under general motion has been largely neglected by the research community. As an exception, a method for mosaicing the pictorial content painted on right circular cylinders was presented in [14]. That method requires that internal camera parameters are known in advance. The external orientation parameters and the imaged symmetry axis are obtained from two imaged circular cross sections. As the method does not fully exploit prior knowledge about scene geometry, pictorial surface

elements cannot be metrically sampled in the warping step, and geometric distortions are introduced. This may affect significantly the subsequent alignment step and the visual quality of the obtained mosaic.

In this paper, a novel approach is presented for the creation of mosaics from collections of uncalibrated perspective views of a Surface of Revolution (SOR). A projective model of SOR scene geometry based on homologies is used both to calibrate each single view and to align metrically the corresponding surface pictorial content from each view according to a translational motion model. The original contribution of this work is two-fold. First, the approach extends previous literature on curved surfaces to the broad class of SOR objects. Second, calibration information need not be known in advance, but can be obtained directly from SOR scene geometry. Experimental results with images taken from the web demonstrate the effectiveness and the general applicability of the approach. In particular, the visual quality of the results is comparable with the one obtained with expensive 3D laser scanning technologies (see e.g. [9]) typically used for cultural heritage applications.

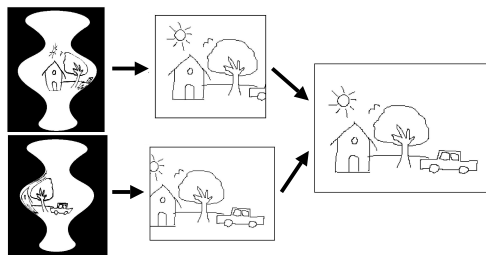


Figure 1: Mosaicing from two SOR images.

2 The Approach

Fig. 1 shows an example of mosaic creation from two SOR views. The imaged SOR surface regions visible from each view (Fig. 1, left) are first individually mapped onto a reference plane (Fig. 1, middle), whereon they can be aligned together and merged into a single mosaic image (Fig. 1, right).

The mosaicing approach consists of three main steps. In the first step, the imaged SOR geometry of each view is estimated from the visible segments of two imaged cross sections, and used to compute the internal camera parameters. The imaged SOR geometry is then exploited together with the calibration information and the imaged SOR silhouette to obtain, for each view, a SOR parameterization common to all the views up to a translation (second step). This removes the projective distortion due to the image formation process, and allows the imaged SOR regions visible from each view to be warped onto a common reference plane. In the final step (alignment and compositing), the unknown translation for each warped image is estimated by region-based image registration, and used to create the mosaic image. In the following sections, each of the steps above will be described in detail.

2.1 Imaged SOR Geometry and Camera Calibration

A SOR can be parameterized as $\mathbf{P}(\theta, z) = (\rho(z) \cos(\theta), \rho(z) \sin(\theta), z)$, where $\theta \in [0, 2\pi]$ and $z \in [0, 1]$. The scaling function $\rho(z)$ controls the 3D shape of the SOR. (In the special case of constant $\rho(z)$, the SOR reduces to the right circular cylinder addressed in [14].) The perspective projection of a SOR gives rise to two different kinds of image curves, namely

the *apparent contour* and the *imaged cross sections*. The former is the image of the points at which the surface is smooth and the projection rays are tangent to the surface; the shape of this curve is view dependent. On the other hand, imaged cross sections are view independent elliptical curves, that correspond to parallel coaxial circles in 3D and arise from surface normal discontinuities or surface texture content. Both the apparent contour and the imaged cross sections of a SOR are transformed onto themselves by a 4-dof harmonic homology $H = \mathbb{I} - 2\frac{\mathbf{v}_\infty \mathbf{l}_s^T}{\mathbf{v}_\infty^T \mathbf{l}_s}$, where \mathbf{l}_s and \mathbf{v}_∞ are respectively the imaged axis of revolution and the vanishing point of the normal direction of the plane passing through \mathbf{l}_s and the camera center [13]. These geometric entities are strictly related to the calibration matrix K , which embeds information about the internal camera parameters. In particular it holds $\mathbf{l}_s = \omega \mathbf{v}_\infty$, where $\omega = K^{-T} K^{-1}$ is the image of the absolute conic [7]. Moreover, since cross sections are parallel circles in 3D, they intersect at the circular points of the families of planes orthogonal to the SOR symmetry axis. Their projection in the image, \mathbf{i} and \mathbf{j} , are also related to the image of the absolute conic as $\mathbf{i}^T \omega \mathbf{i} = 0$ and $\mathbf{j}^T \omega \mathbf{j} = 0$. The resulting system

$$\begin{cases} \mathbf{i}^T \omega \mathbf{i} = 0 \\ \mathbf{j}^T \omega \mathbf{j} = 0 \\ \mathbf{l}_s = \omega \mathbf{v}_\infty \end{cases} \quad (1)$$

provides four linear constraints on ω , whose coefficients can be computed from two imaged ellipses as shown in [4] [5]. A symbolic representation of the geometrical relationships involved in Eq. 1 is shown in Fig. 2(a). It can be demonstrated that only three out of the four constraints above are actually independent. Therefore, the system of Eq. 1 can be used to calibrate a natural camera (zero skew and known aspect ratio: 3 dofs) from a single image.

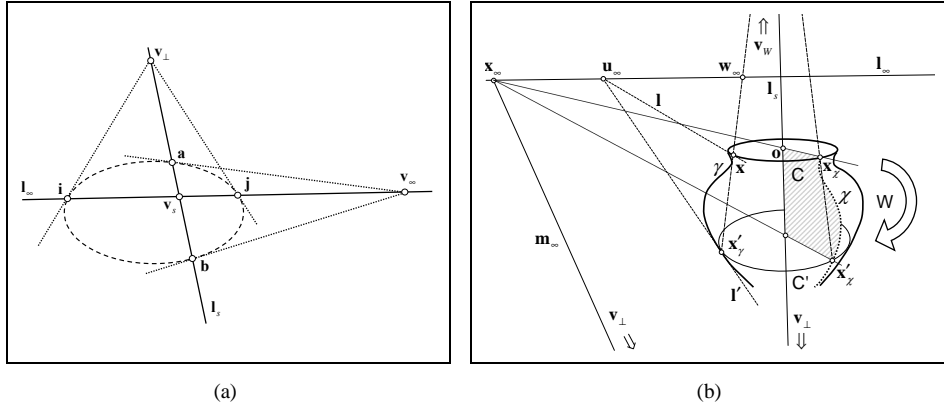


Figure 2: (a): A symbolic representation of the geometry of camera calibration. The IAC is shown dashed to remind that it is a pure imaginary conic. (b) The geometry of imaged SOR parametrization.

2.2 Imaged SOR Parameterization

The image of any SOR point can be backprojected uniquely onto the coaxial right cylinder $(\cos(\theta), \sin(\theta), z)$; this, in turn, can be unrolled onto the plane (θ, z) used as reference plane for mosaicing. The imaged SOR parametrization just described is nothing but the (unknown) warping transformation connecting the image and the mosaicing planes. This section shows how to evaluate the imaged SOR parametrization from the imaged SOR geometry introduced in the previous section and the apparent contour. The following three properties hold (see Fig. 2(b) for a graphical interpretation):

<p>Objective:</p> <ul style="list-style-type: none"> Given $C, \mathbf{l}_\infty, \mathbf{l}_s, \mathbf{v}_\infty$ and $\mathbf{x}'_\gamma \in \gamma$. Compute the imaged cross section C' tangent at \mathbf{x}'_γ. <p>Algorithm:</p> <ol style="list-style-type: none"> 1. Compute the tangent line l' at $\mathbf{x}'_\gamma \in \gamma$. 2. $\mathbf{u}_\infty = l' \times \mathbf{l}_\infty$ 3. Compute $\mathbf{x} \in C$ at which the tangent line l is incident with \mathbf{u}_∞. 4. $\mathbf{v}_W = (\mathbf{x} \times \mathbf{x}'_\gamma) \times \mathbf{l}_s$ 5. $\mathbf{w}_\infty = (\mathbf{x} \times \mathbf{x}'_\gamma) \times \mathbf{l}_\infty$ 6. $\mu_W = \{\mathbf{v}_W, \mathbf{w}_\infty, \mathbf{x}, \mathbf{x}'_\gamma\}$ 7. $W = I + (\mu_W - 1) \frac{\mathbf{v}_W \mathbf{l}_\infty^T}{\mathbf{v}_W^T \mathbf{l}_\infty}$ 8. $C' = W^{-T} C W^{-1}$.
--

Table 1: Computation of the imaged cross section C' tangent to an assigned point \mathbf{x}'_γ on the apparent contour γ . (see Fig.2(b))

Property 2.1 *The apparent contour is tangent to an imaged cross section at any point of contact [1].*

Property 2.2 *The lines tangent to two distinct imaged cross sections C and C' at any two points \mathbf{x} and \mathbf{x}' are related by the planar homology $W = I + (\mu - 1) \frac{\mathbf{v} \mathbf{l}_\infty^T}{\mathbf{v}^T \mathbf{l}_\infty}$ as $\mathbf{x}' = W\mathbf{x}$, and have the same vanishing point \mathbf{u}_∞ , which lies on the vanishing line \mathbf{l}_∞ of all the planes orthogonal to the SOR symmetry axis. The point \mathbf{v} lies on \mathbf{l}_s .*

Property 2.3 *The 3D points whose images $\mathbf{x} \in C$ and $\mathbf{x}' \in C'$ are related as $\mathbf{x}' = W\mathbf{x}$ belong to the same SOR meridian $\theta = \text{constant}$.*

With reference to Fig.2(b), the cross section C' is tangent to the apparent contour γ and the point \mathbf{x}'_γ is the contact point of property 2.1. The line l' tangent at \mathbf{x}'_γ meets \mathbf{l}_∞ at \mathbf{u}_∞ . The line l passing by \mathbf{u}_∞ and tangent to C gives the point \mathbf{x} . The points \mathbf{x} and \mathbf{x}'_γ correspond under the homology W of property 2.3, while l' and l are the tangent lines of property 2.2. The properties above are used in the algorithms shown in Tables 1, 2(a), 2(b) and 3 to solve the imaged SOR parametrization problem. The algorithms in Tab. 3 is the top-most algorithm performing image transformation by using the algorithms in Tabs. 1, 2(a), 2(b). The algorithm in Tab. 1 computes the imaged cross section C' tangent at γ at its generic point $\mathbf{x}'_\gamma \in \gamma$ by transforming a visible cross section C . The inputs $\mathbf{l}_\infty, \mathbf{l}_s, \mathbf{v}_\infty$ are computed from two visible cross section as described in [4]. This algorithm allows one to “move” projectively along imaged cross sections. In particular Tab. 2(a) and 2(b) show how to index a generic imaged surface element with a unique value of θ and z respectively.

Solving for the Euclidean θ . The angle between two lines in a world plane π can be computed in the image in terms of the vanishing points of the lines and the imaged circular points of the plane as shown in Fig. 3(a). In the figure, the Euclidean (world angle) θ between the two imaged lines \mathbf{l}_θ and \mathbf{l}_s can be calculated by the Laguerre’s formula [6]

$$\theta = \frac{1}{2i} \log(\{\mathbf{v}_\theta, \mathbf{v}_s, \mathbf{i}, \mathbf{j}\}) , \quad (2)$$

where $\{\}$ denotes the usual cross ratio of four points [16]. In order to obtain an imaged point at a given θ in a generic imaged cross section C , the Eq. 2 is inverted. By expressing the generic point on the vanishing line \mathbf{l}_∞ of π as $\mathbf{v}(\lambda) = \mathbf{i} + \lambda(\mathbf{i} - \mathbf{j})$, Eq. 2 can be rewritten as

$$e^{i2\theta} = \{\lambda_\theta, \lambda_s, \lambda_i, \lambda_j\} , \quad (3)$$

where λ_θ , λ_s , $\lambda_i = 0$ and $\lambda_j = -1$ are the values of the complex parameter λ respectively for the points \mathbf{v}_θ , \mathbf{v}_s , \mathbf{i} and \mathbf{j} . Given the imaged axis of revolution $\mathbf{l}_s = (l_1, l_2, l_3)$ and the imaged circular points $\mathbf{i} = \text{conj}(\mathbf{j}) = (a + ib, c + id, 1)$, by solving for λ_s the equation $\mathbf{l}_s^T \mathbf{v}(\lambda_s) = 0$ we get $\lambda_s = -\frac{1}{2} [1 + i \tan \phi_s]$, where

$$\phi_s = \arctan \left(-\frac{l_1 a + l_2 c + l_3}{l_1 b + l_2 d} \right). \quad (4)$$

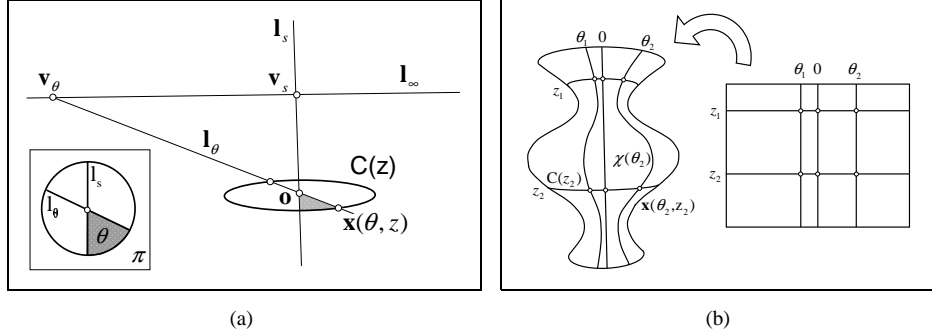


Figure 3: (a) Sampling an imaged cross section $C(z)$ at a given Euclidean angle θ . (b) The texture transformation.

By replacing the above value of λ_s into Eq. 3, the value of λ_θ can be computed as

$$\lambda_\theta = -\frac{1}{2} [1 + i \tan(\phi_s + \theta)] , \quad (5)$$

which yields the vanishing point as $\mathbf{v}_\theta = \mathbf{i} + \lambda_\theta(\mathbf{i} - \mathbf{j})$. The image line $\mathbf{l}_\theta = \mathbf{v}_\theta \times \mathbf{o}$ —where $\mathbf{o} = C^{-1}(z)\mathbf{l}_\infty$ is the image of the cross section center—intercepts the imaged parallel C at two points, of which the required point $\mathbf{x}(\theta, z)$ on the visible imaged meridian $\chi(\theta)$ is the farthest one from \mathbf{v}_θ along the line \mathbf{l}_θ . Tab. 2(a) summarizes the described algorithm.

Solving for the metric z . For any given θ , the algorithms of Tab. 1 and Tab. 2(a) can be used to obtain the whole imaged meridian $\chi(\theta)$. The z value associated to each of the points of this imaged meridian can be obtained by rectification of the plane π_χ through the meridian. The rectifying homography [10] can be computed from the image of the absolute conic ω and the vanishing line \mathbf{m}_∞ of the plane π_χ as $M_r = \begin{pmatrix} \beta^{-1} & -\alpha\beta^{-1} & 0 \\ 0 & 1 & 0 \\ m_1 & m_2 & 1 \end{pmatrix}$, where $\mathbf{m}_\infty = (m_1, m_2, 1)$ and $\mathbf{i}_\chi = \text{conj}(\mathbf{j}_\chi)$ is expressed as $M_r^{-1}(1, i, 0) = (\alpha - i\beta, 1, -m_2 - m_1\alpha + im_1\beta)$. The vanishing line \mathbf{m}_∞ is obtained as $\mathbf{m}_\infty = \mathbf{x}_\infty \times \mathbf{v}_\perp$ (see Fig. 2(b)), where \mathbf{x}_∞ and \mathbf{v}_\perp are respectively the vanishing point of the θ -direction of all lines in π_χ that are orthogonal to the symmetry axis, and the vanishing point of the direction of the symmetry axis. The imaged circular points are computed as the intersection of \mathbf{m}_∞ with ω . As the SOR symmetry axis lies by construction on π_χ , once the rectifying homography M_r for this plane is known, we are able to rectify both the imaged meridian χ and the imaged axis of symmetry \mathbf{l}_s , thus obtaining the required value of z .

The correspondence between a point of the apparent contour $\mathbf{x}'_\gamma \in \gamma$ at which the imaged cross section is tangent-contact and the (normalized) metric z where the 3D cross-section resides can be expressed in terms of a function $\zeta : \gamma \rightarrow [0, 1]$ such that

$$z = \zeta(\mathbf{x}'_\gamma) . \quad (6)$$

Objective: Given an angle θ in the world space, the fixed entities $\mathbf{L}_\infty, \mathbf{l}_s, \mathbf{v}_\infty, \mathbf{i}, \mathbf{j}$ and the conic C . Compute the imaged point $\mathbf{x} \in C$ subtending an angle θ with respect to the plane through the camera center and the 3D axis of revolution.

Algorithm:

1. Compute λ_θ as in Eq. 5
2. $\mathbf{v}_\theta = \mathbf{i} + \lambda_\theta(\mathbf{i} - \mathbf{j})$.
3. $\mathbf{v}_s = \mathbf{l}_s \times \mathbf{l}_\infty$
4. $\mathbf{l}_\theta = \mathbf{v}_\theta \times (C^{-1}\mathbf{l}_\infty)$
6. Intersect C with \mathbf{l}_θ and choose from the two solutions the farthest from \mathbf{v}_θ .

(a)

Objective: Given z compute its corresponding point $\mathbf{x}'_\gamma \in \gamma$ at which the cross section at z is tangent contact to \mathbf{x}'_γ

Algorithm:

0. Set $t_- = 0$ and $t_+ = 1$.
1. Choose t as the midpoint of $[t_-, t_+]$ and set $\mathbf{x}'_\gamma = \gamma(t)$.
2. Compute $\hat{z} = \zeta(\mathbf{x}'_\gamma)$.
3. If $|z - \hat{z}| < \Delta z$ stop.
4. If $z > \hat{z}$ set $t_- = t$; else set $t_+ = t$; go to 1.

(b)

Table 2: (a) Imaged cross section sampling at a given θ . (b) Iterative evaluation of the point on the apparent contour γ that lies at a given z .

Objective:

- Compute the flattened imaged SOR region T

Algorithm:

1. Choose a reference imaged parallel C .
2. Compute $\mathbf{x}'_\gamma = \zeta^{-1}(z)$ and the relative imaged cross section $C(z)'$ with the algorithm of Tab. 2(b).
3. Sample $C(z)'$ at $\theta = \theta_1, \dots, \theta_N$ with the algorithm of Tab. 2(a).
4. For each of the N points $\mathbf{x}'_{\gamma(\theta)} = \mathbf{x}(\theta, z)$ thus obtained, set $T(\theta, z) = I(\mathbf{x}'_{\gamma(\theta)})$.
5. Texture acquisition is achieved by repeating the steps 1 through 4 for all the rows of the texture image T , sampled at regular intervals of z .

Table 3: Texture transformation algorithm.

An algorithm for the computation of $\mathbf{x}'_\gamma = \zeta^{-1}(z)$ at the generic z by successive approximations is outlined in Tab. 2(b). This algorithm is essential for image warping by inverse texture sampling. The unknown \mathbf{x}'_γ is denoted as $\gamma(t)$, where $t \in [0, 1]$ is any curve parameter on γ such that $\zeta(\gamma(0)) = 0$. Hence, the problem can be reformulated as to find the value of t which satisfies $\zeta(\gamma(t)) = z$. The algorithm exploits the fact that the function $(\zeta \circ \gamma)(t)$ is monotonic.

We are now finally in the position to perform image warping according to the algorithm of Tab. 3. The algorithm performs flattened texture acquisition by resampling the original image starting from an orthogonal grid of θ and z values in the reference plane. The image to reference plane transformation maps imaged SOR meridians and parallels onto mutually orthogonal straight lines (see also Fig. 3(b)). It is worth noticing that, to guarantee that texture details have the same size in all the warped images, a unique scaling factor for z must be specified for all the views. In order to achieve this, the portions of apparent contour used to warp each image must be chosen so that they are delimited by two imaged cross sections corresponding to the same 3D SOR parallels in all views. If the SOR has a top and a bottom, these two extremities can be conveniently selected to delimit the apparent contour in each view.

2.3 Texture Alignment

Thanks to the characteristics of the image warping algorithm just described, the subsequent image alignment phase is greatly simplified, and reduced to the problem of estimating rigid translations in the reference plane. The alignment procedure is very similar to that used for cylindrical panoramic mosaics [18]. Both a horizontal translation δ_θ and a vertical translation δ_z are estimated for each input image. Translations along z must be taken into account to



Figure 4: (a) shows the computed imaged meridians at $\theta=10^\circ, 20^\circ, 30^\circ, 40^\circ, 50^\circ, 60^\circ$ measured from the imaged axis of revolution. (b) shows the flattened texture obtained with the described algorithms. Here imaged cross sections and meridians are warped as mutually orthogonal straight lines. (c) Four complementary views of a Japanese vase and the warped flattened textures obtained.

compensate for misalignments due to slight uncertainties in the scaling factor.

Direct registration is employed to align at subpixel accuracy the warped images and recover the translation $\delta = (\delta_\theta, \delta_z)$. The intensity error $E(\delta) = \sum_{x_i} [I_1(x_i + \delta) - I_2(x_i)]^2$ between the two images I_1 and I_2 is minimized using the iterative method described in [11]. The algorithm starts from an initial guess lying close to the minimum.

3 Experimental Results

Fig. 4(a) shows an uncalibrated view of a vase taken from the web. In the figure, two ellipses were manually fitted by following two boundaries corresponding to imaged cross sections. The apparent contour was manually drawn and modeled by an interpolating cubic spline curve. The same figure shows six imaged meridians computed with the described algorithm at increasing angles of 10° measured from the imaged axis of revolution. The imaged meridians shown are part of the resampling grid. The imaged axis of revolution is also the image of a meridian, and specifically the one contained in the plane through the camera center and the 3D axis of revolution. It is worth noticing how the meridian gives the perception of the depth while approaching the apparent contour. The regular sampling of the spline parameter clearly does not induce a regular sampling for the imaged meridians.

The flattened texture of Fig.4(b) is obtained by resampling the curves of the imaged SOR parameterization and warping them onto mutually orthogonal straight lines in the reference texture image (row and column). The largest amount of warping is required by the imaged surface regions close to the apparent contour and by high curvature surface parts. Fig. 4(c) shows four views of the vase of Fig. 4(a) having a common overlapping imaged surface pictorial content. Fig. 4(c) shows also the warped imaged surface in overlapping order. The resolution of the original images is 400×600 . We chose a similar resolution for the warped texture images. Fig. 5(a) shows the manual initialization of the alignment step with three of the four warped images of Fig. 4. Notice how length ratios are maintained in all images, while the lighting is remarkably different from image to image. Fig. 5(b) shows the mosaic image resulting after image alignment and compositing. The mosaic represents a full 360°



Figure 5: (a) Initial guess for the direct registration. (b) The complete mosaic obtained by image registration and compositing.

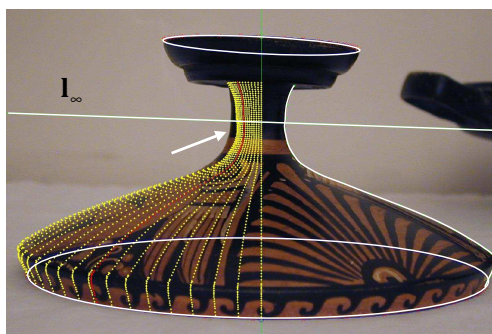
“vase panorama” obtained using five warped images, of which the leftmost image of Fig. 4(c) was used twice in order to close the visual texture loop. The effect of image compositing is to reduce the lighting gradient inside the mosaic. The registration fails when the SOR deviates from its ideal geometry. Fig. 6(a) shows a vase cover in which the axis of revolution is not straight. Since the top cross section is not perfectly coplanar with the bottom one, the generated imaged parameterization is not perfectly registered. The subsequent image alignment cannot be performed under this condition, since the common overlapping regions are different.

The transformations relating the different coordinate system of each imaged SOR region depends on camera calibration. Bad estimates of internal camera parameters can prevent the alignment with the translational motion model. One of the main limitations of this approach is that the quality of the boundary fitting of the ellipses (imaged visible cross sections) strongly affects the accuracy of calibration results. Fig. 6(b) shows the mean and the relative RMS errors in the computation of the principal point (upper) and focal length (lower) for different noise levels corrupting the imaged cross sections of a synthetic SOR view. The influence of this noise was tested by running a Monte Carlo simulation with 10000 trials for each of the parameters under test. Both ellipses and the system of eq.1 are estimated using algebraic distance. Bold curves indicate a reference condition where all the points of the imaged cross sections are available while light curves indicate the condition where only the visible points of the imaged cross section are used. It can be noticed that, in noisy conditions, the accuracy obtained when a subset of the points of the imaged cross sections are used approximates the accuracy that is obtained in the case in which all the points are available.

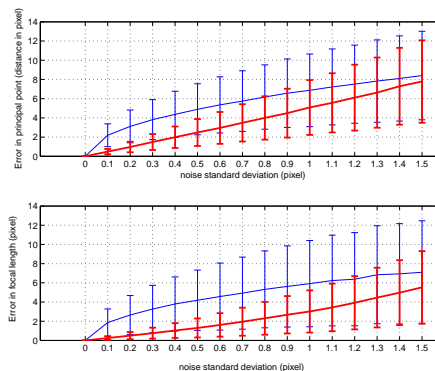
4 Conclusion

In this paper we have discussed a novel method for mosaicing several uncalibrated views of a SOR. The proposed solution exploits the projective properties of SORs class and their relationships with camera geometry. The method uses as inputs two at least partially visible imaged cross sections and the apparent contour (see [3] for an automatic method to extract simultaneously such curves and the imaged geometry).

The method gives good results especially with smooth SORs, and can be used reliably in all those cases in which uncalibrated photographs are available and structured light or other hardware solutions cannot be employed. In particular, the method can be applied for cultural heritage or archaeological objects that are either no more available as original, or cannot be moved from their site. It can also be applied in those cases where the nature of the object material makes it impossible or expensive the acquisition with laser-based techniques [9]. The



(a)



(b)

Figure 6: (a): A vase cover slightly deviating from an ideal SOR. The top cross section is not coplanar with respect to the bottom one. As indicated by the arrow the superimposed parameterization is not perfectly registered. (b): Shows the means and the relative RMS error in the computation of the principal point (upper) and focal length (lower) for different noise level of a synthetic SOR view. The two curves on each graph shows the effect of using only the visible points of the imaged cross section (light curve) or all the points of the cross sections (bold curve).

flattened (rolled-out) representation can be regarded as a virtual painting drawn by the artist onto a curved support. Rolling out this kind of images facilitates the study and comparison of similar images. Specifically, existing image retrieval techniques can be applied for indexing databases of 3D objects by their pictorial surface content.

The main limitations of the method are related to self-occlusions and non smooth SORs, as only the texture portions corresponding to a differentiable apparent contour can be warped. Currently, images are warped separately, and then registered together: this means that calibration errors in one view can affect the final mosaic quality. To reduce the effect of calibration errors, future research will address performing the warping and alignment steps simultaneously. Further improvements will be the use of multiview calibration and the detection and removal of specular highlights.

References

- [1] Samer M. Abdallah. *Object Recognition via Invariance*. PhD thesis, The University of Sydney, Australia, June 2000.
- [2] S. E. Chen. Quicktime vr – an image-based approach to virtual environment navigation. *Computer Graphics (SIGGRAPH'95)*, pages 29–38, August 1995.
- [3] C. Colombo, A. Del Bimbo D. Comanducci, and F. Pernici. Accurate automatic localization of surfaces of revolution for self-calibration and metric reconstruction. *IEEE Workshop on Perceptual Organization in Computer Vision (POCV '04)*. In association with the *IEEE CVPR '04*, June 2004.
- [4] C. Colombo, A. Del Bimbo, and F. Pernici. Uncalibrated 3D metric reconstruction and flattened texture acquisition from a single view of a surface of revolution. *Proc. 1st International Symposium on 3D Data Processing, Visualization, and Transmission (3DPTV'02)*, pages 277–284, 2002.

- [5] C. Colombo, A. Del Bimbo, and F. Pernici. Metric 3d reconstruction and texture acquisition of surfaces of revolution from a single uncalibrated view. *IEEE Transactions on Pattern Analysis and Machine Intelligence*, to appear 2004.
- [6] Olivier Faugeras and Quan-Tuan Luong. *The Geometry of Multiple Images*. The MIT press Cambridge, Massachusetts London, England, 2001.
- [7] R. I. Hartley and A. Zisserman. *Multiple View Geometry in Computer Vision*. Cambridge University Press, 2000.
- [8] M. Irani and P. Anandan. All about direct methods. In W. Triggs, A. Zisserman, and R. Szeliski, editors, *International Workshop on Vision Algorithms: Theory and Practice*, pages 267–277. Springer Verlag, 1999.
- [9] Taylor J., Beraldin J-A., Godin G., Cournoyer L., Baribeau R., Rioux M., and J. Domey. Nrc 3d imaging technology for museum and heritage applications. *Journal of Visualization and Computer Animation*, 14(3):121–138, July 2003.
- [10] D. Liebowitz, A. Criminisi, and A. Zisserman. Creating architectural models from images. In *Proc. EuroGraphics*, volume 18, pages 39–50, September 1999.
- [11] B. Lucas and T. Kanade. An iterative image registration technique with an application to stereo vision. In *Proc. of IJCAI*, pages 674–679, 1981.
- [12] L. McMillan and G. Bishop. Plenoptic modeling: An image-based rendering system. *Computer Graphics (SIGGRAPH'95)*, pages 39–46, August 1995.
- [13] J. Mundy and A. Zisserman. Repeated structures: Image correspondence constraints and ambiguity of 3D reconstruction. In J. Mundy, A. Zisserman, and D. Forsyth, editors, *Applications of invariance in computer vision*, pages 89–106. Springer-Verlag, 1994.
- [14] W. Puech, A.G. Bors, I. Pitas, and J.-M. Chassery. Projection distortion analysis for flattened image mosaicing from straight uniform generalized cylinders. *Pattern Recognition*, 34(8):1657–1670, Aug 2001.
- [15] R. Szeliski. Video mosaics for virtual environments. *IEEE Computer Graphics and Application*, pages 22–30, March 1996.
- [16] J. Semple and G. Kneebone. *Algebraic projective geometry*. Oxford University Press, 1952.
- [17] Hong Shen, Charles V. Stewart, Badrinath Roysam, Gang Lin, and Howard L. Tanenbaum. Frame-rate spatial referencing based on invariant indexing and alignment with application to online retinal image registration. *IEEE PAMI*, 25(3):379–384, march 2003.
- [18] H.-Y. Shum and R. Szeliski. Systems and experiment paper: Construction of panoramic mosaics with global and local alignment. *IJCV*, 36(2):101–130, February 2000.
- [19] S. Peleg, B. Rousso, A. Rav-Acha, and A. Zomet. Mosaicing on adaptive manifolds. *IEEE PAMI*, 22(10):1144–1154, October 2000.
- [20] P. H. S. Torr and A. Zisserman. Feature based methods for structure and motion estimation. In W. Triggs, A. Zisserman, and R. Szeliski, editors, *International Workshop on Vision Algorithms: Theory and Practice*, pages 278–295. Springer Verlag, 1999.